A High-Sensitivity Fiber-Optic Fabry-Perot Gas Pressure Sensor With Epoxy Resin Adhesive

Danping Xu, Haitao Gao, Zheyu Hou, Yanan Zhang, Xuanxiang Tong, Yizhuo Zhang, Pengyu Zhang, Jian Shen, and Chaoyang Li

***Abstract*—A high-sensitivity fiber-optic gas pressure sensor based on a Fabry-Perot interferometer filled with epoxy resin adhesive is proposed. The factors of affecting the pressure sensitivity are theoretically analyzed and verified experimentally. In our experiment, the pressure sensitivity of the epoxy-filled sensor with the thinnest diaphragm thickness of 6.61 μm corresponding to the cavity length of 65.45 μm is −530.17 pm/kPa from 200 to 300 kPa. The sensitivity of the proposed pressure sensor with the shortest cavity length of 90.43 μm corresponding to the film thickness of 10.65 μm is −378.18 pm/kPa from 200 to 300 kPa. To further improve the sensitivity, the proposed pressure sensor is optimized, which consists of two cascaded Fabry-Perot interferometers separated by a long section of single-mode fiber to form Vernier effect. Such a pressure sensor based on the epoxy-filled Fabry-Perot interferometer and the Vernier effect obtains a high sensitivity of 2.526 nm/kPa in the local measurement range of 233 to 259 kPa and a low detection limit of 0.00892 kPa. With the advantages of high sensitivity, compact structure and simple fabrication, the proposed pressure sensor has potential applications in the biomedical field and ocean exploration.**

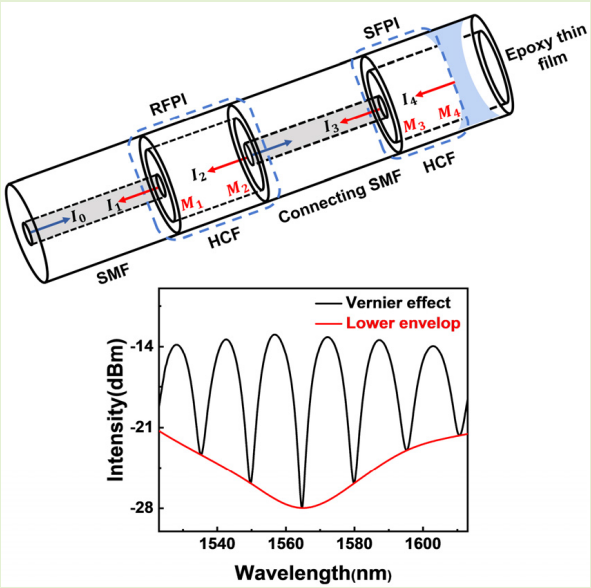

***Index Terms*—Fabry-Perot interferometer, epoxy resin adhesive, fiber-optic gas pressure sensor, Vernier effect.**

I. Introduction

PRESSURE is one of the most basic physical parameters, and real-time measurement and monitoring of pressure is of great significance to daily life and engineering application. Fiber-optic Fabry-Perot interferometric (FPI) pressure sensor, with outstanding advantages of flexible configuration, compact structure, miniature size as well as immunity to electromagnetic interference [1]–[4], is widely applied to various fields of biomedicine [5], aerospace industries [6], and down-hole oil/gas exploration [7].

Manuscript received April 2, 2022; accepted April 14, 2022. Date of publication April 18, 2022; date of current version May 31, 2022. This work was supported in part by the Hainan Provincial Natural Science Foundation of China under Grant 2019RC054, in part by the Finance Science and Technology Project of Hainan Province under Grant ZDKJ2020009, and in part by the Sichuan Science and Technology Program under Grant 2021ZYD0033. The associate editor coordinating the review of this article and approving it for publication was Dr. Minghong Yang. *(Danping Xu and Haitao Gao contributed equally to this work.) (Corresponding authors: Jian Shen; Chaoyang Li.)*

The authors are with the School of Information and Communication Engineering and the State Key Laboratory of Marine Resource Utilization in South China Sea, Hainan University, Haikou 570228, China (e-mail: xudanping@hainanu.edu.cn; gaohaitao@hainanu.edu.cn; shenjian@hainanu.edu.cn; lichaoyang@hainanu.edu.cn).

Digital Object Identifier 10.1109/JSEN.2022.3168290

The sensing principle of FPI pressure sensor is based on changing the optical path difference or the reflectance of interference cavity surfaces, which are associated with Fabry-Perot (F-P) cavity length, refractive index and reflectance. The typical FPI pressure structure is that the material film with a certain elasticity replaces one of the reflective surfaces of interference cavity, such as silica [8], polymer [9], [10] graphene [11], and water [12]. With the diaphragm's elastic deformation principle, the film reflective surface is deformed under pressure, thereby changing the F-P cavity length. The deformation degree of the film is related to the Young's modulus of the material itself. The lower the Young's modulus of the material, the greater the elastic deformation of the diaphragm and the higher the pressure sensitivity.

An adhesive-based FPI pressure sensor has been reported, the F-P cavity of which is formed by the polymerized resin between two single-mode fiber (SMF) terminals [9]. M. Yao *et al.* presented a miniature fiber-tip sensor based on the μ-printed polymer suspended-microbeams, which exhibited a pressure sensitivity of 4.29 nm/MPa [13]. However, the formation of the F-P cavity and the control of the thickness of the reflective surface involve a complex preparation process. C. R. Liao *et al.* demonstrated a silica diaphragm-based

fiber-tip FPI sensor [14]. The fabrication process is simple, only using electrical arc discharge technique. However, the pressure sensitivity is low only 1036 pm/MPa and still needs to be improved. Q. S. Cui *et al.* investigated a FPI structure formed by exfoliated ultrathin graphene atomic layer as a reflective surface, which achieved a high pressure sensitivity of 1.28 nm/mmHg [11]. However, the graphene structure is not strong enough to be used in demanding conditions. Therefore, the diaphragm-based FPI sensor, with the design of sensor structure, the selection of film material, the optimization of fabrication process, and the enhancement of the sensitivity, still need to be explored and demonstrated continuously.

Epoxy resin adhesive is an elastomeric polymer, which is selected as the material of the pressure sensitive film owing to the excellent characteristics of good elasticity, low cost, and strong adhesive strength. High elasticity, corrosion resistance, and water resistance make epoxy-based FPI pressure sensor promising for the medical treatment and ocean exploration. In addition, some materials, such as PDMS requires baking at least 6 hours at 70 °C to complete curing [10]; UV adhesive must be cured by irradiated under UV light for 20 min [15]. In comparison, epoxy resin adhesive only needs to stand for 24 h at room temperature.

In this paper, a highly sensitive pressure sensor based on the epoxy-filled FPI structure is proposed, which is fabricated by welding a short section of hollow-core fiber (HCF) to the SMF, and filling a thin layer of epoxy film at the end face of the HCF under capillary action. Furthermore, the methods to effectively improve the pressure sensitivity have been theoretically analyzed and demonstrated experimentally, with a maximum pressure sensitivity of 2.526 nm/kPa and a low detection limit of 0.00892 kPa. The designed sensor with high sensitivity is compact, easy-fabrication, cost effective, and is suitable for practical sensing applications.

II. Structure Fabrication and Sensing Principle

A. Epoxy-Filled FPI Gas Pressure Sensor

The preparation process of the sensor probe is as follows. Firstly, a section of the SMF (Corning SMF28e+) and the HCF (Polymicro Technologies, TSP075150, with a core diameter of 75 μm, and a cladding diameter of 150 μm), are spliced by a commercial welding machine (Fujikura, Tokyo, Japan, 80C+), as shown in Fig. 1a. In the fusion splicing process, appropriate welding parameters must be employed to avoid collapse of the air-cavity. The discharge power and the discharge time are set as −85 bit and 1200 ms, respectively. Second, the HCF is cleaved with a certain length on the precision-cutting platform displayed in Fig. 1b. The preparatory work before the third step is the preparation of epoxy resin adhesive by mixing a precursor of elastic polymer and the hardener with the ratio of 1:1 and stirring well. Then, we use the SMF with flat end face to dip a small amount of epoxy glue, and then make it contact with HCF back and forth in the welding machine until the epoxy glue into the HCF end face to form an epoxy film, as shown in Fig. 1c. If the diaphragm formed is thick, we can use another SMF with flat and clean end face to contact the film again to absorb the excess epoxy glue. On the contrary, the film thickness can be increased by using a common SMF to inject a suitable amount of epoxy glue into the sensor probe. Finally,an epoxy-filled FPI structure is obtained exhibited in Fig. 1d. The fabricated epoxy-filled FPI structure needs to be left at room temperature for 24 h to cure completely.

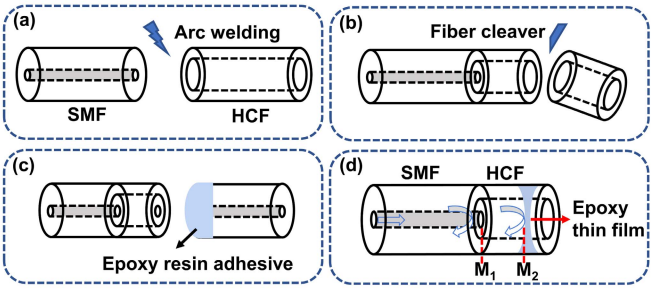

Fig. 1. Fabrication process of the proposed pressure sensor. (a) The welding of SMF and HCF. (b) The cutting of the HCF. (c) The process of the epoxy glue injection. (d) The structure of epoxy-filled FPI.

The proposed epoxy-filled FPI pressure sensor is composed of an enclosed F-P microcavity, the two reflective surfaces of which are formed by the end face of the SMF (M_1) and the internal surface of the epoxy diaphragm (M_2). The incident light is coupled into fiber core and partially reflected when it reaches two surfaces to form interference. The wavelength dip of the reflection spectrum can be defined as [16]:

$$\lambda_m = \frac{4nL}{2m+1} \tag{1}$$

where n is the air refractive index of 1, and L is the length of the F-P air-cavity. m is an integer and represents the order of the interference fringes.

The F-P cavity length can be calculated as [17]:

$$L = \frac{\lambda_1 \lambda_2}{2n(\lambda_1 - \lambda_2)} \tag{2}$$

whereλ_1 and λ_2 are the wavelengths corresponding to adjacent peaks or valleys in the measured interference spectrum.

The wavelength spacing between adjacent peaks or valleys is called as free spectral range (FSR), which can be calculated as [18]:

$$FSR = \frac{\lambda_1 \lambda_2}{2nL} = \frac{\lambda_0^2}{2nL} \tag{3}$$

whereλ_0 is the mean wavelength of λ_1 and λ_2. According to (3), the FSR of the interference spectrum decreases as the L increases when n remains unchanged.

With the variation of external gas pressure, the deformation of the diaphragm causes the change of cavity length and interference spectrum. The relationship between the pressure change ΔP and cavity length change ΔL can be expressed as [10]:

$$\Delta L = \frac{(1-\mu)\cdot r^2}{2Ed} \cdot \Delta P \tag{4}$$

where μ is the Poisson ratio of the film; r is diaphragm's effective radius, that is, the inner radius of the HCF; E is the

Young' s modulus of the diaphragm; d is the thickness of the film. The Poisson's ration and Young's modulus of epoxy resin adhesive are about 0.25 and 2.5 MPa, respectively.

The wavelength offset of the reflectance spectrum with pressure changing is as follows [19]:

$$\Delta\lambda_m = \lambda_m \cdot \frac{\Delta L}{L} \tag{5}$$

The ratio of wavelength shift to pressure change is defined as the pressure sensitivity [10].

$$Y = \frac{\Delta\lambda_m}{\Delta P} = \frac{\lambda_m \cdot (1-\mu) \cdot r^2}{2LEd} \tag{6}$$

Due to the epoxy resin adhesive selected as diaphragm material, the Poisson ratio and the Young' s modulus are constants, so the pressure sensitivity is only related to F-P cavity length, diaphragm thickness, and effective radius. According to (6), the pressure sensitivity is inversely proportional to membrane thickness and F-P cavity length, and is proportional to effective radius. The shorter the F-P cavity length, the thinner the film thickness, and the larger the effective radius, the higher the sensitivity of the diaphragm-based pressure sensor. However, the increase of the effective radius can lead to an increase in sensor size. Hence, thinning the thickness of the membrane or reducing the F-P cavity length are two effective methods to improve the sensitivity.

B. Pressure Sensor With Separated Cascaded FPI Structures Based on the Vernier Effect

By the theoretical analysis above mentioned, the pressure sensitivity can be increased by the film thickness or shortening the F-P cavity length. Nevertheless, on account of the difficulty of preparation process, the reduction of diaphragm thickness and F-P cavity length are limited. Consequently, for the sake of greater sensitivity, the optimized pressure sensor based on the Vernier effect is proposed exhibited in Fig. 2, which is formed by combination of two cascaded air-cavity FPIs separated by a section of connecting SMF. The epoxy-filled FPI structure is used as the sensing FPI(SFPI), and another air-cavity is used as the reference FPI(RFPI). The RFPI is fabricated by sandwiching a section of HCF between the lead-in SMF and the caudal SMF displayed in Fig. 3.

Unlike the common cascaded-cavity structure of the Vernier FPI sensor, the proposed sensor utilizes a section of connecting SMF to separate the RFPI from the SFPI. The separated cascaded FPIs structure thus consists of four reflective surfaces (M_1 and M_4), and each pair of reflective surfaces forms a F-P cavity. Specifically, the air-cavity RFPI is formed between M_1 and M_2; the connecting SMF between M_2 and M_3 forms a silica-cavity $FPI_{M_2M_3}$; the air-cavity SPFI is formed between M_3 and M_4; and any two nonadjacent reflecting surfaces form hybrid cavities $FPI_{M_1M_3}$, $FPI_{M_1M_4}$, and $FPI_{M_2M_4}$. If the connecting SMF is long enough, then it only serves to transmit light and there will be not multiple single FPIs and multiple hybrid FPIs. Therefore, the length of the connecting SMF must be set appropriately. In our experiment, the length of the connecting SMF is about 2 cm. In this case, only the RPFI and SFPI contribute to the total interference spectrum of the proposed Vernier sensor. Hence, the four reflective surfaces are simplified as the superposition of the reflectance spectra of the two separated FPIs (RPFI and SFPI). The total reflection spectrum of the proposed sensor can be described as [17]:

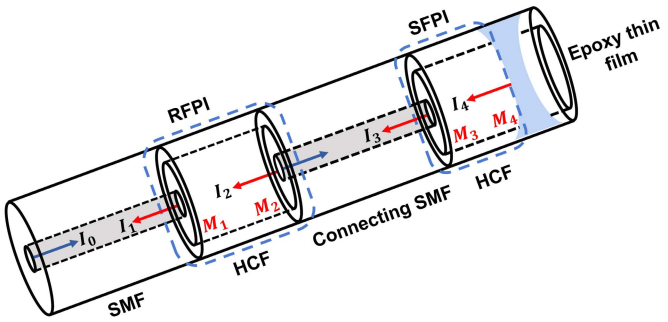

Fig. 2. Structure of the optimized pressure sensor composed of two separated cascaded FPIs.

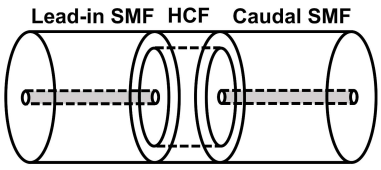

Fig. 3. Structural representation of the RFPI.

$$I = I_1 + I_2 + I_3 + I_4 + 2\sqrt{I_1 I_2}\cos(\frac{4\pi n L_R}{\lambda}) + 2\sqrt{I_3 I_4}\cos(\frac{4\pi n L_s}{\lambda}) \tag{7}$$

where I_1, I_2, and I_4 are the intensities of the four reflective surfaces M_1, M_2, M_3, and M_4, respectively; L_R and L_S are the cavity lengths of the RFPI and the SFPI.

To generate the Vernier effect, the FSRs of two FPIs need to be very close to, but not completely equal to, each other. This can be realized by adjusting the cavity lengths of two FPIs, as both FPIs are air cavities which have the same refractive index. With the Vernier effect, the pressure response characteristics are obtained by measuring the envelope shift formed by cascaded superposition spectrum. The FSR of the spectral envelop is much larger than that of a single FPI is as follows [20]:

$$FSR_{envelop} = \frac{FSR_R \cdot FSR_S}{|FSR_R - FSR_S|} \tag{8}$$

where FSR_R, FSR_S, and $FSR_{envelop}$ are the FSRs of the RFPI, SFPI, and the envelop of the Vernier effect, respectively.

The spectral envelope excursion of the Vernier effect can be expressed as [21]:

$$\Delta\lambda_{envelop} = \Delta\lambda_m \cdot \frac{FSR_R}{|FSR_R - FSR_S|} \tag{9}$$

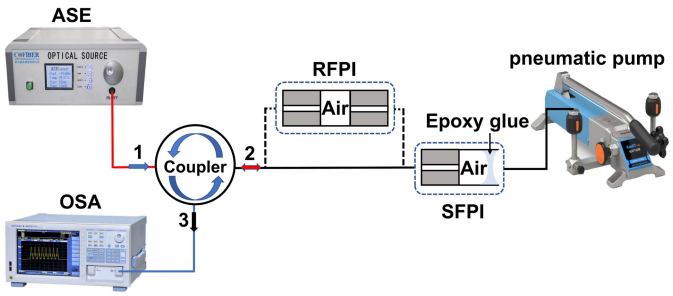

Fig. 4. Experimental setup of gas pressure measurement.

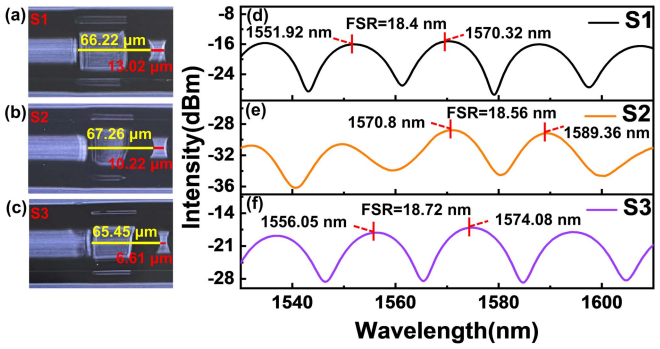

Fig. 5. (a)–(c) The micrographs of different film thickness sensor samples. (d)–(f) Reflectance spectra corresponding to different sensor samples at 200 kPa.

The pressure sensitivity can be greatly improved by tracing the wavelength shift of the spectral envelop.

$$Y_{envelop} = \frac{\Delta\lambda_{envelop}}{\Delta P} = \frac{\Delta\lambda_m}{\Delta P} \cdot \frac{FSR_R}{|FSR_R - FSR_S|} = M \cdot \frac{\Delta\lambda_m}{\Delta P} \tag{10}$$

M is defined as the magnification of the pressure sensitivity expressed by the follow formula [20]:

$$M = \frac{FSR_R}{|FSR_R - FSR_S|} \tag{11}$$

III. Sensor Performance Testing and Analysis

The schematic diagram of the gas pressure detection device is illustrated in Fig. 4. The epoxy-filled FPI structure (SFPI) is first connected to the experimental setup for pressure measurement, and the RFPI is temporarily suspended. The fabricated samples are placed in the air chamber and sealed with strong adhesive. The air chamber can be pressurized linearly by manually adjusting the pneumatic pump at room temperature. The incident light from an amplified spontaneous emission (ASE, with the spectrum region ranging from 1530 to 1610 nm) broadband light source is coupled to the sensor head via a fiber-optic circulator. The reflected light is then collected by an optical spectrum analyzer (OSA, with the resolution of 0.1 nm) to continuously monitor the resulting interference pattern.

According to the theoretical analysis, the pressure sensitivity of the proposed diaphragm-based sensor can be improved by reducing F-P cavity length or film thickness. Therefore, we experimentally demonstrated the feasibility of these two methods for increasing the pressure sensitivity.

A. Pressure Sensitivities of Different Film Thicknesses Based on the Epoxy-Filled FPI

For the first method, we fabricated three sensors with different diaphragm thicknesses but the same F-P cavity length (named as S1, S2, and S3). Fig. 5(a)-(c) show that the film thicknesses of the three fabricated sensors are 13.02 μm, 10.22 μm, and 6.61 μm, respectively, and the corresponding F-P cavity lengths are about 66 μm. Fig. 5(d)-(f) exhibit the reflectance spectra of three sensing samples at 200 kPa, and

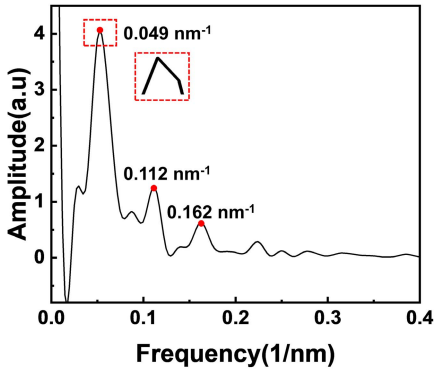

Fig. 6. The spatial frequency spectrum of S1.

the measured FSRs are 18.4 nm, 18.56 nm, and 18.72 nm in turn.

The spatial frequency spectrum of S1 obtained by fast Fourier transform (FFT) is shown in Fig. 6. There are three particularly distinct frequency peaks, labeled Peak 1(0.049 nm^{-1}), Peak 2(0.112 nm^{-1}), and Peak 3 (0.162 nm^{-1}). There are two reasons for the appearance of the Peak 2 and Peak 3. One is that three reflective surfaces interfere with each other, and the other is that the Peak 2 and the Peak 3 are the harmonics of the Peak 1. The proposed sensor contains three F-P cavities. Specifically, the end face of the SMF and the inner surface of the epoxy film form an air cavity (C1). The epoxy diaphragm forms a polymer cavity. The third F-P cavity (C3) is a hybrid cavity formed by the end face of the SMF and the external surface of the epoxy film. The spatial frequencies for three F-P cavities C1, C2, and C3 are calculated as [22] $f_1 = 2nL/\lambda^2$, $f_2 = 2n_{epoxy}l/\lambda^2$, and $f_3 = 2(nL + n_{epoxy}l)/\lambda^2$, where n_{epoxy} (~1.45) is the RI of epoxy and l is the thickness of the epoxy. By taking the wavelength of 1560 nm, the theoretical calculated values for f_1, f_2, and f_3 are 0.054 nm^{-1}, 0.016 nm^{-1}, and 0.069 nm^{-1}. The experimental frequency value of Peak 1 agrees well with the calculated frequency value of C1. This reveals that C1 cavity is the main contributor to the high frequency interference fringes. The Peak 2 and Peak 3 are the second and the third harmonics of the Peak 1, respectively. The C2 cavity has little influence on the spectrum. The inflection point

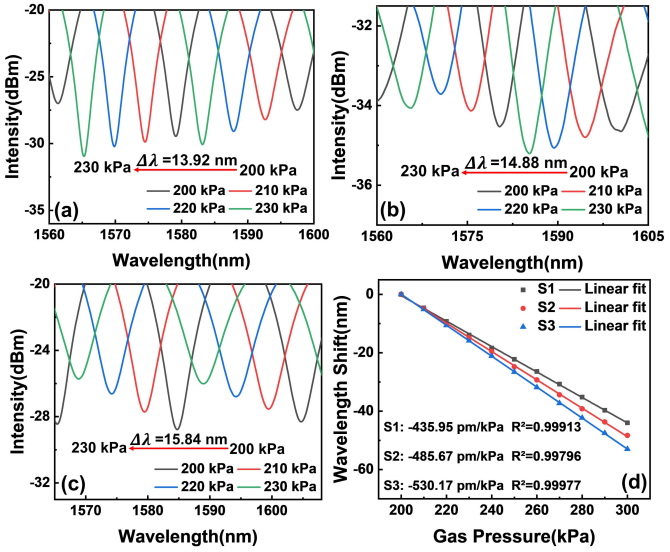

Fig. 7. (a)–(c) Local amplification of spectral shifts of different film thickness sensors ranging from 200 to 230 kPa. (d) Linear fitting curves of the pressure sensitivities ranging from 200 to 300 kPa.

near the top of Peak 1 may be due to the mixing of C1 and C3 cavities, thereby resulting in uneven spectra. In addition, we tested the maximum bearing pressure range of S3 with the film thickness of 6.61 μm. The pressure is continuously increased from 0 kPa. When the pressure exceeds 400 kPa, the spectrum is deformed. Compared with spectral peaks, the fringe dips offer a lower full width at half-maximum (FWHM) and better resolution, as shown in Fig. 5(d)-(f). Thus, we use the dips of the spectra to track the wavelength shift. As can be seen from Fig. 7(a)-(c), the interference dips of three sensor samples occur significant blue shift with the pressure increased from 200 to 230 kPa, and the corresponding spectral offsets are 13.92 nm, 14.88 nm, and 15.84 nm, respectively. Fig. 7d displays that the pressure sensitivities of three different film thickness sensors are −435.95 pm/kPa, −485.67 pm/kPa, and −530.17 pm/kPa, respectively, with the pressure ranging from 200 to 300 kPa at a step of 10 kPa. The theoretical pressure sensitivity of S1 near 1590 nm calculated by (6) is −389 pm/kPa. The sensitivity error may be caused by inaccurate proportion of elastic polymer and hardener. According to the laboratory findings, the sensor with a thinner membrane achieves a higher pressure sensitivity, which is consistent with our previous theoretical analysis.

B. Pressure Sensitivities of Different F-P Cavity Lengths Based on the Epoxy-Filled FPI

Another way of improving the sensitivity of the FPI pressure sensor is to reduce F-P cavity length. Hence, we also fabricated three sensors with different cavity lengths but the same membrane thickness (named as S4, S5, and S6). The micrographs of three different F-P cavity length sensors are exhibited in Fig. 8(a)-(c). The cavity lengths of three different sensors are 163.74 μm, 104.8 μm, and 90.43 μm, respectively, and the film thicknesses are about 10.7 μm. Fig. 8(d)-(f) manifest the corresponding reflection spectra of three sensors

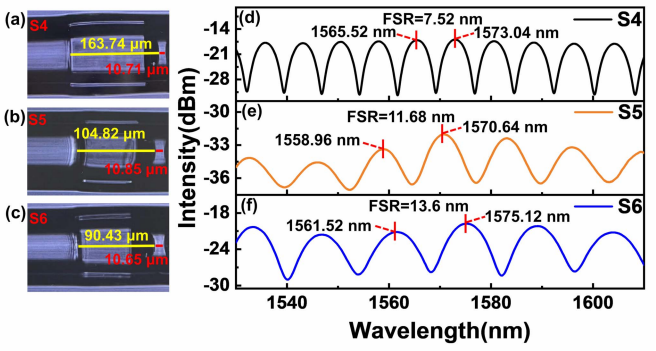

Fig. 8. (a)–(c) The micrographs of different cavity length sensors. (d)–(f) Reflectance spectra corresponding to different sensor samples at 200 kPa.

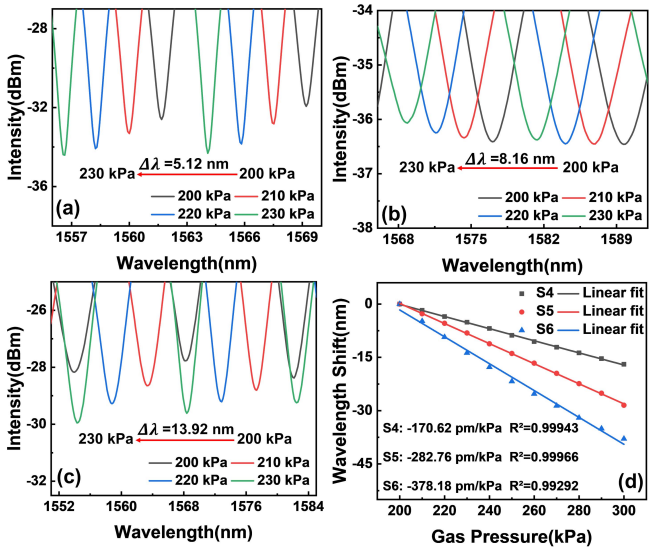

Fig. 9. (a)–(c) Local amplification of spectral shifts of different cavity length sensors ranging from 200 to 230 kPa. (d) Linear fitting curves of the pressure sensitivities ranging from 200 to 300 kPa.

at 200 kPa, and the FSRs of the interference spectra are 7.52 nm, 11.68 nm, and 13.6 nm. The FSR increases with the cavity length decreases, which is consistent with the description of (2). Fig. 9(a)-(c) show that the corresponding wavelength drifts for three different sensors are 5.12 nm, 8.16 nm, and 13.92 nm ranging from 200 to 230 kPa. When the pressure rises from 200 to 300 kPa with a gradient of 10 kPa, the pressure sensitivities of three different cavity length sensors are −170.62 pm/kPa, −282.76 pm/kPa, and −378.18 pm/kPa, respectively, as shown in Fig. 9d. The experimental result is in complete agreement with the previously mentioned theory, which has proven that a shorter F-P cavity length contributes to a higher pressure sensitivity.

The temperature response of the proposed FPI structure was also investigated without applied external pressure. The sensor sample of S5 was placed on the heating table (with an accuracy of 0.1 °C) where the temperature was increased from 40 to 80 °C. Fig. 10a exhibits that the reflection spectrum drifts slightly towards the long wave direction as rising temperature. The relationship between wavelength shift and

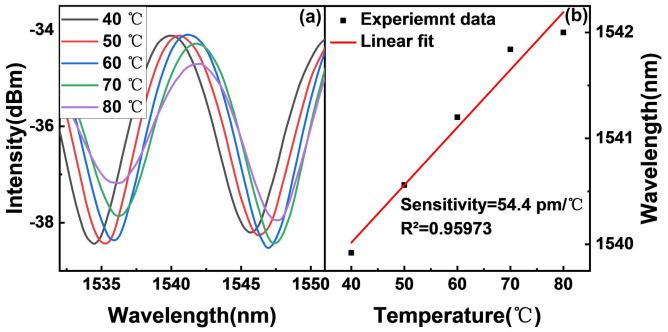

Fig. 10. (a) The temperature response characteristic of S5. (b) Linear fitting of dip wavelengths versus temperature.

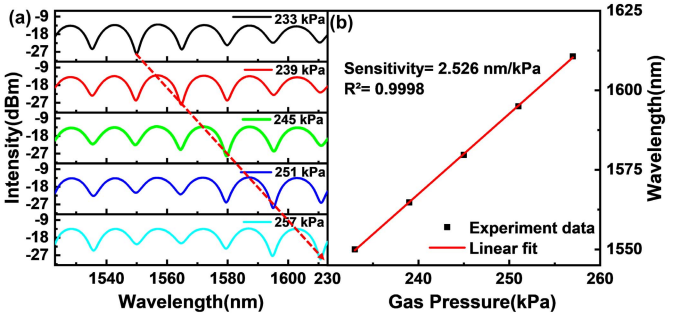

Fig. 12. (a) Gas pressure response of separated cascaded FPIs based on Vernier effect increasing from 233 to 257 kPa. (b) The relationship of the resonate wavelength and pressure.

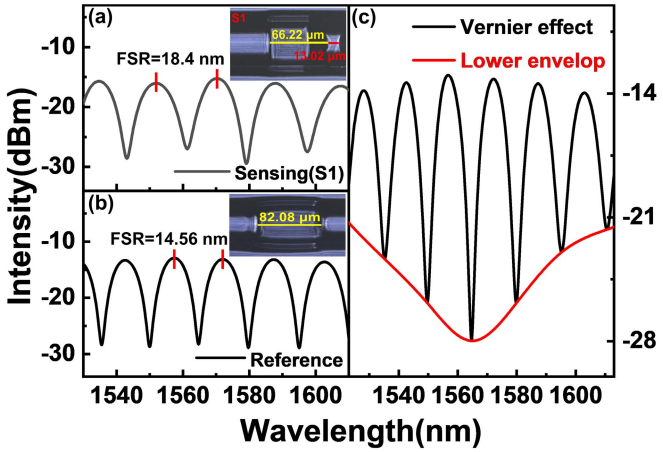

Fig. 11. Reflectance spectra of (a) the SFPI and (b) the RFPI. (c) Interference spectrum and the corresponding lower envelope with the Vernier effect.

increasing temperature is plotted in Fig. 11b that displays a linear variation with a temperature sensitivity of 54.4 pm/°C. The measured temperature response demonstrates that the temperature sensitivity of such an epoxy-based FPI is mainly determined by the thermal expansion effect of the epoxy, and the calculated temperature cross-sensitivity of S5 is 0.192 kPa/°C at atmosphere pressure. Being limited by our lab conditions, the temperature responses for different pressures have not been tested. However, it is believed that the temperature sensitivity and the temperature cross-sensitivity for different pressure both increase with the increase of pressure due to the reduction of the F-P cavity length [23]. In addition, in our previous work [24], it can be concluded that humidity has a minor influence on the proposed epoxy-based FPI sensor in a specific range of humidity changes.

C. Pressure Sensitivity of Separated Cascaded FPI Structures Based on the Vernier Effect

In order to further improve the sensitivity on the basis of the epoxy-filled FPI sensor, an optimized pressure sensor based on the Vernier effect formed by separated cascaded FPIs, is proposed and experimentally demonstrated. Fig. 11(a)-(b) displays the reflectance spectra of the SFPI(S1) and the RFPI, and the corresponding FSRs are 18.4 nm and 14.56 nm. On account of the similar FSRs of the SFPI and RFPI, Vernier effect can be generated. The lower envelop of the Vernier effect is made up of many sine waves with different intensities revealed in Fig. 11c. The FSR of the envelop is about 69.77 nm, which is much larger than that of the single SFPI. As the pressure increases from 200 to 300 kPa, only wavelength shift of the local pressure measurement range can be detected owing to the limited bandwidth of the device. Therefore, a partial pressure scope of 233 to 257 kPa is chosen to ensure that the entire envelop excursion is within the range of observation. With the pressure rising from 233 to 257 kPa with 6 kPa intervals, the envelop curve is redshifted in the opposite direction of the SFPI, as shown in Fig. 12a. The envelop shift based on the Vernier effect is determined by the difference between the $FSR_S$and FSR_R. When the FSR_S is smaller than FSR_R, the envelop drift is consistent with that of the SFPI, and vice versa. Fig. 12b indicates that the pressure sensitivity of the sensor with the Vernier effect is 2.526 nm/kPa, and the wavelength shift and pressure keep good linearity of 0.9998. Compared with a single epoxy-filled FPI, the pressure sensitivity of the Vernier effect structure is magnified 5.79 times, which is similar to the theoretical value ($M = 4.79$), and the calculated detection limit of the sensor is 0.00892 kPa. The sensitivity of pressure-drop is 2.529 nm/kPa, and the linearity is 0.99983 shown in Fig. 13. The experimental results manifest that the sensor has good repeatability. In the process of lowering the pressure ranging from 300 to 200 kPa, the envelop happens a slight drift due to the instability of the experimental equipment and the disturbance of the external environment. Furthermore, we only concatenate the RFPI to the test system during the experiment and make no change to the SFPI. Therefore, the function of the RFPI can be regarded as the modulation effect on the sensing signal. The performances of the sensing probe remain unchanged, only the signal is modulated by the RFPI.

The comparison of the pressure sensing performance between our proposed sensor and other various types of FPI structures is summarized in Table I. Based on the table, the proposed sensor probe exhibits a higher pressure sensitivity compared with other sensors. Therefore, our proposed FPI sensor is suitable for high sensitivity pressure measurement. Whereas, the proposed sensor still has some shortcomings. As the membrane is thinner, it is not strong enough to

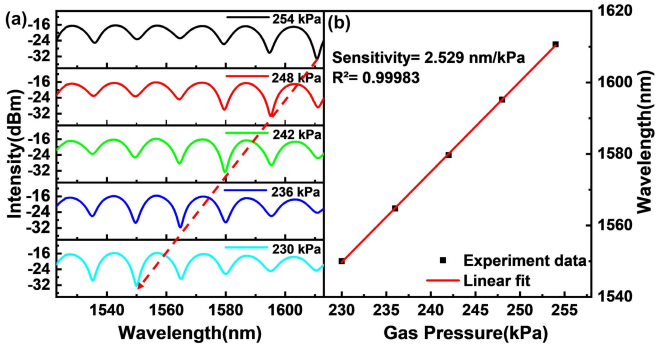

Fig. 13. (a) Gas pressure response of separated cascaded FPIs based on the Vernier effect decreasing from 254 to 230 kPa. (b) The relationship of the resonate wavelength and pressure.

TABLE I
COMPARISON OF SENSING PERFORMANCES OF THE PROPOSED SENSOR WITH REPORTED SCHEMES

FPI Structure	Range(kPa)	Sensitivity(pm/kPa)	Ref.
Silicon microbubble	0-1600	6.79	[25]
PDMS microcavity	100-700	52.143	[10]
Silica hollow microbubble	92-140	164.56	[26]
PVC diaphragm-based FPI	0-60	65.5	[27]
UV-filled/Vernier effect	100-700	-38.3	[15]
Epoxy-filled/Vernier effect	233-257	2526	This work

withstand high pressure and is awfully easy to cause damage to the sensor. If the diaphragm is increased to a certain extent, there will be hybrid FPI that make signal demodulation more difficulty. When the Vernier effect is introduced to our designed pressure sensor, the increased sensitivity comes at the expense of pressure measurement range. Because of the limited wavelength bandwidth of the laboratory equipment, wavelength offset over a larger pressure measurement range cannot be monitored.

IV. CONCLUSION

In conclusion, this work proposed and experimentally demonstrated an ultrasensitive fiber-optic gas pressure sensor based on the epoxy-filled FPI structure. The pressure sensitivities of the sensor probes with the thinnest diaphragm thickness and the shortest F-P cavity length are −530.17 pm/kPa and −378.18 pm/kPa, respectively. To further improve sensitivity, we make the epoxy-filled FPI cascade an F-P air cavity separated by a section of connecting SMF to form Vernier effect, and the optimized FPI structure obtains a higher sensitivity up to 2.526 nm/kPa. The proposed pressure sensor exhibits the advantages of high sensitivity, easy manufacturing and low cost, which can provide a competitive candidate for practical applications.

REFERENCES

[1] W. P. Chen, D. N. Wang, B. Xu, C. L. Zhao, and H. F. Chen, "Multimode fiber tip Fabry–Pérot cavity for highly sensitive pressure measurement," *Sci. Rep.*, vol. 7, no. 1, p. 368, Dec. 2017, doi: 10.1038/s41598-017-00300-x.

[2] Y. Liu *et al.*, "Simultaneous measurement of gas pressure and temperature with integrated optical fiber FPI sensor based on in-fiber microcavity and fiber-tip," *Opt. Fiber Technol.*, vol. 46, pp. 77–82, Dec. 2018, doi: 10.1016/j.yofte.2018.09.021.

[3] Z. Li, J. Tian, Y. Jiao, Y. Sun, and Y. Yao, "Simultaneous measurement of air pressure and temperature using fiber-optic cascaded Fabry–Pérot interferometer," *IEEE Photon. J.*, vol. 11, no. 1, pp. 1–10, Feb. 2019, doi: 10.1109/JPHOT.2018.2884776.

[4] B. Xu, Y. Liu, D. Wang, D. Jia, and C. Jiang, "Optical fiber Fabry–Pérot interferometer based on an air cavity for gas pressure sensing," *IEEE Photon. J.*, vol. 9, no. 2, pp. 1–9, Apr. 2017, doi: 10.1109/JPHOT.2017.2685939.

[5] B. Romner and P.-O. Grände, "Intracranial pressure monitoring in traumatic brain injury," *Nature Rev. Neurol.*, vol. 9, no. 4, pp. 185–186, Apr. 2013, doi: 10.1038/nrneurol.2013.37.

[6] M. J. Gander *et al.*, "Embedded micromachined fiber-optic Fabry–Pérot pressure sensors in aerodynamics applications," *IEEE Sensors J.*, vol. 3, no. 1, pp. 102–107, Feb. 2003, doi: 10.1109/JSEN.2003.810099.

[7] J. M. Ward, N. Dhasmana, and S. Nic Chormaic, "Hollow core, whispering gallery resonator sensors," *Eur. Phys. J. Special Topics*, vol. 223, no. 10, pp. 1917–1935, Sep. 2014, doi: 10.1140/epjst/e2014-02236-5.

[8] X. Cheng, J. Dash, D. Gunawardena, L. Htein, and H.-Y. Tam, "Silicone rubber based highly sensitive fiber-optic Fabry–Pérot interferometric gas pressure sensor," *Sensors*, vol. 20, no. 17, p. 4927, Aug. 2020, doi: 10.3390/s20174927.

[9] R. Oliveira, L. Bilro, R. Nogueira, and A. M. Rocha, "Adhesive based Fabry–Pérot hydrostatic pressure sensor with improved and controlled sensitivity," *J. Lightw. Technol.*, vol. 37, no. 9, pp. 1909–1915, May 1, 2019, doi: 10.1109/JLT.2019.2894949.

[10] X. Wei *et al.*, "Optical fiber gas pressure sensor based on polydimethylsiloxane microcavity," *J. Lightw. Technol.*, vol. 39, no. 9, pp. 2988–2993, May 1, 2021, doi: 10.1109/JLT.2021.3054883.

[11] Q. Cui, P. Thakur, C. Rablau, I. Avrutsky, and M. M.-C. Cheng, "Miniature optical fiber pressure sensor with exfoliated graphene diaphragm," *IEEE Sensors J.*, vol. 19, no. 14, pp. 5621–5631, Jul. 2019, doi: 10.1109/JSEN.2019.2904020.

[12] Y. Wang, D. N. Wang, C. Wang, and T. Hu, "Compressible fiber optic micro-Fabry–Pérot cavity with ultra-high pressure sensitivity," *Opt. Exp.*, vol. 21, no. 12, p. 14084, Jun. 2013, doi: 10.1364/OE.21.014084.

[13] M. Yao, X. Ouyang, J. Wu, A. Zhang, H.-Y. Tam, and P. Wai, "Optical fiber-tip sensors based on *in-situ* μ-printed polymer suspended-microbeams," *Sensors*, vol. 18, no. 6, p. 1825, Jun. 2018, doi: 10.3390/s18061825.

[14] C. Liao *et al.*, "Sub-micron silica diaphragm-based fiber-tip Fabry–Pérot interferometer for pressure measurement," *Opt. Lett.*, vol. 39, no. 10, p. 2827, May 2014, doi: 10.1364/OL.39.002827.

[15] R. Pan *et al.*, "High-sensitive fiber-optic pressure sensor based on Fabry–Pérot interferometer filled with ultraviolet glue film and Vernier effect," *Opt. Fiber Technol.*, vol. 67, Dec. 2021, Art. no. 102710, doi: 10.1016/j.yofte.2021.102710.

[16] T. Nan *et al.*, "Ultrasensitive strain sensor based on Vernier-effect improved parallel structured fiber-optic Fabry–Pérot interferometer," *Opt. Exp.*, vol. 27, no. 12, p. 17239, Jun. 2019, doi: 10.1364/OE.27.017239.

[17] J. Tian, Z. Li, Y. Sun, and Y. Yao, "High-sensitivity fiber-optic strain sensor based on the Vernier effect and separated Fabry–Pérot interferometers," *J. Lightw. Technol.*, vol. 37, no. 21, pp. 5609–5618, Nov. 1, 2019, doi: 10.1109/JLT.2019.2936174.

[18] J. Wang *et al.*, "Investigation of composite structure with dual Fabry–Pérot cavities for temperature and pressure sensing," *Photonics*, vol. 8, no. 5, p. 138, Apr. 2021, doi: 10.3390/photonics8050138.

[19] S. Zhang *et al.*, "An optical fiber pressure sensor with ultra-thin epoxy film and high sensitivity characteristics based on blowing bubble method," *IEEE Photon. J.*, vol. 13, no. 1, pp. 1–10, Feb. 2021, doi: 10.1109/JPHOT.2021.3055872.

[20] H. Lin, F. Liu, H. Guo, A. Zhou, and Y. Dai, "Ultra-highly sensitive gas pressure sensor based on dual side-hole fiber interferometers with Vernier effect," *Opt. Exp.*, vol. 26, no. 22, p. 28763, Oct. 2018, doi: 10.1364/OE.26.028763.

[21] L. G. Abbas, "Vernier effect based strain sensor with cascaded Fabry–Pérot interferometers," *IEEE Sensors J.*, vol. 20, no. 16, pp. 9196–9201, Aug. 2020, doi: 10.1109/JSEN.2020.2988469.

[22] D. Fu, X. Liu, J. Shang, W. Sun, and Y. Liu, "A simple, highly sensitive fiber sensor for simultaneous measurement of pressure and temperature," *IEEE Photon. Technol. Lett.*, vol. 32, no. 13, pp. 747–750, May 2020, doi: 10.1109/LPT.2020.2993836.

[23] Y. Yu, X. Chen, Q. Huang, C. Du, S. Ruan, and H. Wei, "Enhancing the pressure sensitivity of a Fabry–Pérot interferometer using a simplified hollow-core photonic crystal fiber with a microchannel," *Appl. Phys. B, Lasers Opt.*, vol. 120, no. 3, pp. 461–467, Sep. 2015, doi: 10.1007/s00340-015-6155-4.
[24] Y. Zhang *et al.*, "A high precision fiber optic Fabry–Pérot pressure sensor based on AB epoxy adhesive film," *Photonics*, vol. 8, no. 12, p. 581, Dec. 2021, doi: 10.3390/photonics8120581.
[25] S. Zhang *et al.*, "An optical fiber Fabry–Pérot pressure sensor with optimized thin microbubble film shaping for sensitivity enhancement," *Coatings*, vol. 10, no. 4, p. 358, Apr. 2020.
[26] G. Wang *et al.*, "A high-sensitive pressure sensor using a single-mode fiber embedded microbubble with thin film characteristics," *Sensors*, vol. 17, no. 6, p. 1192, May 2017, doi: 10.3390/s17061192.
[27] Z. Zhang *et al.*, "High-sensitivity gas-pressure sensor based on fiber-tip PVC diaphragm Fabry–Pérot interferometer," *J. Lightw. Technol.*, vol. 35, no. 18, pp. 4067–4071, Sep. 15, 2017, doi: 10.1109/JLT.2017.2710210.

Danping Xu was born in Jiangsu, China, in 1994. She is currently pursuing the master's degree in information and communication engineering with Hainan University. The discipline of her research focuses on the optical fiber sensors.

Haitao Gao is currently pursuing the master's degree in information and communication engineering with Hainan University. His main research interest is optical fiber sensors.

Zheyu Hou is pursuing the Ph.D. degree with the School of Information and Communication Engineering, Hainan University. His research interests include optical fiber sensors and deep learning.

Yanan Zhang is currently pursuing the master's degree in information and communication engineering with Hainan University. Her main research interest is optical fiber sensors.

Xuanxiang Tong is currently pursuing the master's degree in information and communication engineering with Hainan University. His main research interests include optical fiber sensors and surface plasmon resonance sensors.

Yizhuo Zhang is currently pursuing the master's degree in information and communication engineering with Hainan University. His main research interests are in the structural design and theoretical modeling of various types of optical sensors.

Pengyu Zhang is pursuing the Ph.D. degree with the School of Information and Communication Engineering, Hainan University. His research interests include optical fiber sensors and spin Hall effect of light.

Jian Shen received the Ph.D. degree in electronic science and technology from the University of Electronic Science and Technology of China in 2012. He is currently an Associate Professor and a Master's Supervisor of Hainan University. His main research area is optic communication sensing technology.

Chaoyang Li received the Ph.D. degree from the University of California at Berkeley, Berkeley. He worked at the world-renowned Lawrence Berkeley Laboratory. He is currently a Professor and a Doctoral Supervisor of Hainan University. His main research interests are information and sensing chip technology.